

# On the Resonances of a Dielectric BOR Buried in a Dispersive Layered Medium

Norbert Geng, *Member, IEEE*, David R. Jackson, *Fellow, IEEE*, and Lawrence Carin, *Senior Member, IEEE*

**Abstract**—A method-of-moments (MoM) analysis is applied to the problem of determining late-time resonances of dielectric bodies of revolution buried in a lossy layered medium, with application to plastic-land-mine identification. To make such an analysis tractable, we have employed the method of complex images to evaluate the layered-medium Green's function. The application of this method to resonant structures characterized by complex resonant frequencies, introduces numerical issues not manifested at real frequencies (i.e., for driven problems) with such discussed here in detail. Numerical results are presented for several buried targets in which we demonstrate, for example, the spiraling character of the resonant frequencies of particular targets as a function of target depth.

**Index Terms**—Buried object detection, natural resonances, inhomogeneous media.

## I. INTRODUCTION

IF a target is excited by a short pulse of electromagnetic energy, fields are diffracted initially at localized scattering centers in and on the target. Subsequently, after the incident wave has departed (at what is termed "late time"), multiple diffractions occur *between* scattering centers and, for a penetrable target, energy reverberates inside as well. Each such multiple diffraction or reverberation is accompanied by energy that radiates away from the scatterer. Consequently, the late-time energy in and on the target decays, as do the associated late-time radiated fields. This late-time phenomenon has been parametrized rigorously in terms of the well-known singularity expansion method (SEM) developed by Baum [1], in which each resonant mode is associated with a pole in the complex frequency plane. Additionally, Felsen *et al.* [2], [3] have rigorously connected the SEM resonances to multiple late-time diffractions and reverberations.

The SEM resonant frequencies, representative of the natural target response, are independent of excitation (i.e., are aspect independent [1]–[5]), although the strength of excitation of a given mode is excitation dependent. Aspect independence of such resonant frequencies has precipitated significant interest in resonant-frequency-based target *identification*. Resonance-based discrimination has been investigated for airborne [6], [7] as well as subsurface [8], [9] targets, using such techniques as Prony's method [10], [11] and the matrix-pencil method

[12]. In the work presented here, we are interested in dielectric targets (e.g., plastic land mines) buried in a lossy, dispersive layered medium (simulating soil). There have been previous experimental studies on resonance-based identification of plastic targets, with some results being particularly promising [8], [9]. However, it is well known that the strength of excitation of such modes is strongly dependent on the electrical contrast between the dielectric target and the background soil. Moreover, a recent study [13] on the SEM resonances of buried *conducting* targets has revealed an often strong dependence of the resonant frequencies on the target depth. This is because, for subsurface targets, the resonant frequencies are not dictated by the buried target alone, but by the *total* scattering environment (i.e., the target in the presence of the soil). In particular, if there are strong reverberations between the target and air-ground interface, the target depth plays an important role in the total-target resonant frequencies. This is a very important issue, for the target depth is often not known exactly (e.g., for buried mines), complicating resonance-based identification of such targets. Since it is difficult to comprehensively study this issue experimentally, for a wide range of targets, soil types, and target depths, an accurate theoretical model is required, motivating the work presented here.

Modeling of a target's natural modes requires solution of the source-free target response. Therefore, algorithms which require an excitation such as the finite-difference time-domain (FDTD) [14], are inappropriate. While the target resonant frequencies can in principle be extracted from the late-time fields computed via such a time-domain model (via, for example, the Prony [10], [11] or matrix-pencil [12] algorithms discussed above), modal excitation is dictated by the driving function and, therefore, a range of incident fields would be required to catalogue all the modes of a given structure. Consequently, the natural target response is best analyzed with a frequency-domain algorithm. The finite-element method (FEM) [15] constitutes a frequency domain scheme that can be adapted for such purposes. However, while FEM algorithms are quite general and accurate, they require discretization of the fields throughout the computational domain. For the three-dimensional problems of interest here, in complicated layered environments, the generality of FEM is obviated by the attendant numerical complexity [15]. Therefore, here we utilize the method of moments (MoM), with restriction to targets that can be simulated as a body of revolution (BOR); for the layered-medium problem of interest here, the BOR axis is required to be normal to the layer surfaces (Fig. 1), thereby

Manuscript received February 10, 1998; revised June 16, 1999.

N. Geng and L. Carin are with the Department of Electrical and Computer Engineering, Duke University, Durham, NC 27708-0291 USA.

D. R. Jackson is with the Department of Electrical and Computer Engineering, University of Houston, Houston, TX 77204-4793 USA.

Publisher Item Identifier S 0018-926X(99)07959-4.

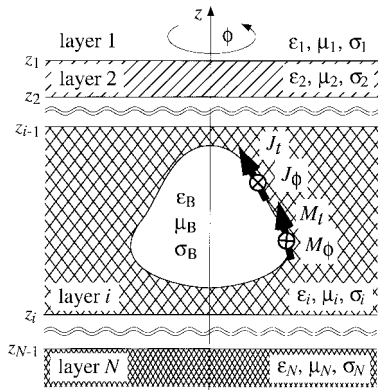


Fig. 1. Schematic of a dielectric body of revolution buried in a layered medium.

preserving rotational symmetry throughout the BOR (layered-medium) composite. While the restriction to BOR targets is clearly a simplification, most land mines are accurately so modeled [16].

The MoM analysis of targets buried in a lossy layered medium requires accurate computation of the layered-medium Green's function with such necessitating the efficient analysis of Sommerfeld spectral integrals [17]–[21]. Numerous techniques have been developed for the analysis of these ubiquitous integrals [17]–[21], with the recently developed method of complex images constituting a particularly attractive option [22]–[25]. This algorithm represents the spectral-domain reflection coefficient inherent to the spectral Green's function in terms of a sum of exponentials, determined via parametric estimation (again, via either of the aforementioned parametric algorithms [10]–[12]). Subsequently, each spectral-domain term in this summation is converted to the space domain analytically, via the Sommerfeld or Weyl identity [26]. The parametric estimation is performed along a proper path in the complex spectral plane with careful consideration of branch cuts and possible surface-wave and leaky-wave poles [27]. While such matters have been addressed in detail for the driven problem, characterized by *real* frequencies, special consideration is required for resonant-frequency computation. In particular, target resonances are characterized by *complex* frequencies, introducing complications with regard to branch-cut and pole locations, with such impacting the path of integration for the Sommerfeld integrals. We address these issues in detail and demonstrate how such are handled within the context of the method of complex images.

The remainder of the text is organized as follows. In Section II we summarize the general features of MoM-based analysis of SEM resonances for dielectric BOR's buried in a lossy, layered medium (e.g., soil). For details on the layered-medium Green's function, recent work on such is cited. However, the application of the method of complex images at resonant (complex) frequencies is new, and is therefore discussed in detail. In Section III, several numerical results are presented as a function of the properties of the target, target depth, and background environment. Finally, conclusions are addressed in Section IV.

## II. NUMERICAL ALGORITHM

### A. Method of Moments Formulation

We are interested in the natural (resonant) modes of a dielectric BOR embedded in a lossy, dispersive layered medium (see Fig. 1). By enforcing boundary conditions for the tangential electric and magnetic field components on the BOR surface, one obtains coupled integral equations for the resonant electric and magnetic surface currents  $\mathbf{J}$  and  $\mathbf{M}$ , respectively. We employ a mixed-potential integral equation (MPIE) formulation from which we have (for *complex*  $\omega = \omega' + j\omega''$ )

$$0 = \mathbf{n} \times \int_S [j\omega\mu(\mathbf{r})\mathbf{K}_A(\mathbf{r}, \mathbf{r}')] + j\omega\mu_B G_B(\mathbf{r}, \mathbf{r}')\mathbf{I}] \cdot \mathbf{J}(\mathbf{r}') dS' - \mathbf{n} \times \nabla \int_S \left[ \frac{K_{\phi\epsilon}(\mathbf{r}, \mathbf{r}')}{\sigma(\mathbf{r}) + j\omega\epsilon(\mathbf{r})} + \frac{G_B(\mathbf{r}, \mathbf{r}')}{\sigma_B + j\omega\epsilon_B} \right] \nabla' \cdot \mathbf{J}(\mathbf{r}') dS' + \mathbf{n} \times \nabla \times \int_S [\mathbf{G}_F(\mathbf{r}, \mathbf{r}') + G_B(\mathbf{r}, \mathbf{r}')\mathbf{I}] \cdot \mathbf{M}(\mathbf{r}') dS' \quad (1a)$$

$$0 = \mathbf{n} \times \int_S [(\sigma(\mathbf{r}) + j\omega\epsilon(\mathbf{r}))\mathbf{K}_F(\mathbf{r}, \mathbf{r}') + (\sigma_B + j\omega\epsilon_B)G_B(\mathbf{r}, \mathbf{r}')\mathbf{I}] \cdot \mathbf{M}(\mathbf{r}') dS' - \mathbf{n} \times \nabla \int_S \left[ \frac{K_{\phi m}(\mathbf{r}, \mathbf{r}')}{j\omega\mu(\mathbf{r})} + \frac{G_B(\mathbf{r}, \mathbf{r}')}{j\omega\mu_B} \right] \nabla' \cdot \mathbf{M}(\mathbf{r}') dS' - \mathbf{n} \times \nabla \times \int_S [\mathbf{G}_A(\mathbf{r}, \mathbf{r}') + G_B(\mathbf{r}, \mathbf{r}')\mathbf{I}] \cdot \mathbf{J}(\mathbf{r}') dS' \quad (1b)$$

where  $\mathbf{I}$  represents the unit dyad. The layered-medium permittivity, permeability, and conductivity are represented by  $\epsilon(\mathbf{r})$ ,  $\mu(\mathbf{r})$ , and  $\sigma(\mathbf{r})$ , respectively, and  $\epsilon_B$ ,  $\mu_B$ , and  $\sigma_B$  represent these same parameters for the homogeneous, lossy BOR target. Electric and magnetic charge densities on the surface have been replaced by derivatives of the electric and magnetic surface current densities, respectively, using the continuity relation. Explicit expressions for the spectral-domain layered-medium dyadic kernel  $\mathbf{K}_A$ , the dyadic Green's function  $\mathbf{G}_A$  (representing the magnetic vector potential produced by an infinitesimal electric dipole), and the electric scalar potential  $K_{\phi\epsilon}$  of a point charge associated with a horizontal electric dipole have been given by Michalski and Zheng [21], where we use their "Formulation C." The additional terms  $\mathbf{K}_F$ ,  $\mathbf{G}_F$ , and  $K_{\phi m}$  are necessitated by the equivalent magnetic currents (not present for perfectly conducting targets [21]) and can be determined via duality. Finally, for calculating the field inside the homogeneous BOR, produced by currents on its surface, we utilize the homogeneous-medium Green's function  $G_B = \exp(-jk_B R)/4\pi R$ , where  $R$  represents the distance between source and observation points and  $k_B$  denotes the wavenumber inside the BOR.

The integral equations in (1) are applicable to any dielectric target embedded in a layered medium, but here we restrict ourselves to the case of a BOR to make the numerical analysis tractable. However, as stated in the Introduction, most plastic land mines, the interest of this work, closely approximate BOR's [16]. The MoM analysis of BOR's in free-space is well known [28], [29], with the integral equations in (1) similar

to such, with substitution of the layered-medium Green's function. Therefore, the principal challenge here involves the efficient analysis of the Green's function components  $\mathbf{K}_A, \mathbf{G}_A, K_{\phi e}, \mathbf{K}_F, \mathbf{G}_F$ , and  $K_{\phi m}$ , necessitating the evaluation of several Sommerfeld-type integrals [17]–[25]. In the subsequent two sections, we address the proper path of integration in the complex spectral plane for the evaluation of such integrals, with application to resonant-frequency calculations. Moreover, we discuss how such integrals are computed efficiently, via a modified form of the method of complex images [22]–[25].

After representation of the surface currents  $\mathbf{J}$  and  $\mathbf{M}$  along the BOR generating arc [29], we generate homogeneous matrix equations (one for each azimuthal mode [28]–[30]) of the form

$$\mathbf{Z}\mathbf{i} = \mathbf{0} \quad (2)$$

where  $\mathbf{Z}$  is an  $N \times N$  MoM impedance matrix and  $\mathbf{i}$  is an  $N \times 1$  vector representing the basis-function coefficients for the  $N$  expansion functions. The impedance matrix is a function of frequency  $\omega$  and nontrivial solutions for  $\mathbf{i}$  occur at frequencies for which the determinant of  $\mathbf{Z}(\omega)$  vanishes, providing a numerical scheme for computation of the complex resonant frequencies. The relative modal currents are computed subsequently [29], [30]. Details on the efficient computation of  $\mathbf{Z}(\omega)$  for dielectric BOR's embedded in a layered medium can be found in [31].

### B. Path of Spectral Integration: Loss-Free Case

The layered-medium Green's function is of interest in a wide range of problems [21], [31] and, therefore, the evaluation of such has constituted an important area of research. As is well known, layered-medium Green's functions can only be evaluated in closed form in the spectral domain with Sommerfeld-type integrals required for determination of their space-domain counterparts. Numerous numerical and analytic techniques [17]–[25] have been devised for the evaluation of such integrals. Here we exploit the method of complex images [22]–[25]. Previous use of the method of complex images has focused primarily on driven problems at *real* frequencies [22]–[25]. For the evaluation of target resonances, of interest here, we seek the natural (nondriven) modes of the structure, which are characterized by *complex* resonant frequencies [30]. We therefore address the evaluation of Sommerfeld integrals at complex frequencies, with subsequent application to the method of complex images. Moreover, to simplify the presentation, the discussion is restricted initially to the case of *lossless* media with a subsequent generalization for inclusion of loss.

We are interested in evaluating integrals of the form

$$f(\xi, z, z') = \frac{1}{2\pi} \int_0^\infty \hat{f}(k_\rho, z, z') J_0(k_\rho \xi) k_\rho dk_\rho \quad (3)$$

where  $\xi = [(x - x')^2 + (y - y')^2]^{1/2}$ . Because our problem is open above and below, branch points exist at  $k_\rho = \pm k_1$  and  $k_\rho = \pm k_N$  [32], where  $k_1$  and  $k_N$  are the wavenumbers for the top (first) and bottom ( $N$ th) layers, respectively. For an

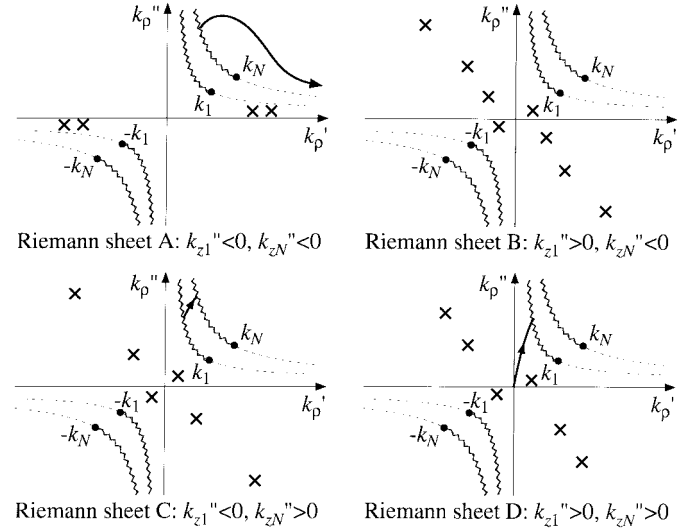


Fig. 2. Four Riemann sheets defined by the choice of branch cuts in (4). The path of integration exists on portions of three sheets, and the crosses denote possible surface- and leaky-wave pole positions. For wavenumbers  $k_{z1} = k'_{z1} + jk''_{z1}$  and  $k_{zN} = k'_{zN} + jk''_{zN}$  (for the first and  $N$ th layer in Fig. 1, respectively), the Riemann sheets are characterized by  $k''_{z1} < 0$  and  $k''_{zN} < 0$  on sheet A,  $k''_{z1} > 0$  and  $k''_{zN} < 0$  on sheet B,  $k''_{z1} < 0$  and  $k''_{zN} > 0$  on sheet C, and  $k''_{z1} > 0$  and  $k''_{zN} > 0$  on sheet D.

assumed  $\exp(j\omega t)$  time dependence, a given complex resonant frequency is of the form  $\omega = \omega' + j\omega''$ , where  $\omega' > 0$  and  $\omega'' > 0$  (characteristic of a damped oscillation). Therefore, the branch points reside in the first and third quadrants of the complex  $k_\rho$  plane (assuming that the wave velocities in regions 1 and  $N$  are real at *complex*, resonant frequencies; the restriction to lossless media implies these velocities are real at *real* frequencies). It is convenient to define branch cuts such that the various surface- and leaky-wave poles are clearly partitioned to particular Riemann sheets [32]. In particular, we utilize the well-known branch cuts [32] defined as (for complex  $k_\rho = k'_\rho + k''_\rho$  and  $k_n = k'_n + jk''_n$ )

$$k'_1 k''_1 = k'_\rho k''_\rho, \quad k_\rho^2 - k_\rho''^2 < k_1'^2 - k_1''^2 \quad (4a)$$

$$k'_N k''_N = k'_\rho k''_\rho, \quad k_\rho^2 - k_\rho''^2 < k_N'^2 - k_N''^2. \quad (4b)$$

The branch cuts in (4a) and (4b) are necessitated by  $k_{z1} = [k_1^2 - k_\rho^2]^{1/2}$  and  $k_{zN} = [k_N^2 - k_\rho^2]^{1/2}$ , respectively, both of which appear in the spectral Green's function (we define  $k_{z1} = k'_{z1} + jk''_{z1}$  and  $k_{zN} = k'_{zN} + jk''_{zN}$ ). These branch cuts result in the four Riemann sheets shown in Fig. 2, where sheets A through D are characterized, respectively, by  $k''_{z1} < 0$  and  $k''_{zN} < 0$ ,  $k''_{z1} > 0$  and  $k''_{zN} < 0$ ,  $k''_{z1} < 0$  and  $k''_{zN} > 0$ , and  $k''_{z1} > 0$  and  $k''_{zN} > 0$ . Recognizing that the fields radiated away in regions 1 and  $N$  are characterized by  $\exp(-jk_{z1}z)$  and  $\exp(jk_{zN}z)$ , respectively, we can attribute physical meaning to the modes (poles) that may exist on each of the four Riemann sheets. (It should be noted that such modes, characterized by poles in the  $k_\rho$  plane, are the waveguide modes supported by the layered medium [32], at a given complex resonant frequency, not the modes of the resonant structure itself; the poles of the resonant structure occur in the complex *frequency* plane [1]). On Riemann sheet

$A$ , the fields decay exponentially with increasing  $z$  in region 1 and with decreasing  $z$  in region  $N$  and, therefore, this surface is characterized by a finite number of poles, representative of surface waves. At the complex frequency characteristic of a resonant mode, the fields *grow* exponentially with transverse distance  $\xi$  away from the source [30] and, therefore, (for an  $\exp(-jk_\rho\xi)$  dependence for large  $\xi$ ) the surface-wave poles reside in the first and third quadrants of Riemann sheet  $A$ .

On Riemann sheet  $B$ ,  $k''_{z1} > 0$  and  $k''_{zN} < 0$ , and, therefore, the layered-medium modes represented by poles on this sheet are characterized by exponential growth with  $z$  in region 1, while decaying exponentially in region  $N$ . This phenomenon is characteristic of a leaky (improper) mode [27], [32], with leakage into region 1. One must be careful to assess the position of these leaky-wave poles in the complex  $k_\rho$  plane. We begin by considering resonant frequencies  $\omega' + j\omega''$  for which  $\omega'' \rightarrow 0$ , characteristic of a very high- $Q$  resonator. This represents the limiting case of nondamped time-harmonic excitation, for which the leaky-wave pole positions are well known [27], [32]. In particular, for the time-harmonic case such modes are characterized by exponential growth in region 1 ( $k''_{z1} > 0$ ), and exponential decay with distance  $\xi$  away from the source ( $k''_\rho < 0$ ) [27], [32], the decay in  $\xi$  manifested by energy lost to leakage. Therefore, under such circumstances, the leaky-wave poles reside in the fourth quadrant of this Riemann sheet (the negatives of these leaky-wave poles also exist, in the second quadrant) [27], [32]. There are an infinite number of such leaky-wave poles [27], [32], with the rate of leakage increasing with increasing  $|k''_\rho|$ . We now consider what happens as  $\omega''$  increases, reflecting a lowering of the resonator  $Q$ . The energy emitted from the resonant source decays with time, with a corresponding growth in energy with distance  $\xi$  from the source [30]. If the rate of leakage is sufficiently small, the spatial growth associated with the radiated resonant energy will overcome the exponential decay in  $\xi$  attributed to leakage and, therefore, such weakly leaky modes are characterized by  $k''_\rho > 0$  (i.e., they grow with  $\xi$ ). Therefore, it is possible that on sheet  $B$ , a *finite* number of leaky-wave poles may exist in the first (and third) quadrant. However, as mentioned above, for the harmonic case the rate of leakage increases with increasing  $|k''_\rho|$  and, therefore, there will be an infinite number of leaky-wave poles for which the rate of leakage overcomes the spatial growth associated with the resonator, leading to leaky-wave fields that decay with  $\xi$  (i.e.,  $k''_\rho < 0$ ); the associated poles of such modes are situated in the fourth (and second) quadrant of the complex  $k_\rho$  plane (as for the case of harmonic excitation).

This phenomenon can be understood by making an analogy to a source in the presence of an active medium that supports leaky waves (e.g., a leaky transmission line [33]–[35] loaded with active elements [36]). In the absence of leakage, the fields on the transmission line grow with distance from the source due to the active elements (corresponding to the resonant fields in the layered media, which grow with distance from the resonator). However, due to leakage, the transmission line mode loses energy with distance. If the rate of leakage exceeds the rate of active-element-induced gain, the fields will decay

with distance from the source, with the opposite true in the case of weak leakage. If, as for the layered medium, there are an infinite number of leaky waves, with increasing rates of leakage, there will only be a finite number of such modes with small enough leakage for the fields to grow with distance from the source, while there are an infinite number of leaky waves for which the rate of leakage exceeds the rate of gain, causing energy decay with distance.

Returning to the layered medium of interest here, we address the other types of leaky waves that can be supported in such a medium [27], [32]. In particular, the poles on Riemann sheet  $C$  are characterized by leakage (exponential growth) into layer  $N$  and exponential decay in region 1, while the poles of Riemann sheet  $D$  are characterized by leakage (exponential growth) into both regions 1 and  $N$ . The leaky-wave pole positions for sheets  $C$  and  $D$  are as discussed above for Riemann sheet  $B$ .

Having detailed the four Riemann sheets of the complex  $k_\rho$  plane, we now address the path of integration for the integral in (3). Recall that on sheet  $D$  the fields are radiated (and grow exponentially) out of regions 1 and  $N$ , on sheet  $C$  the fields decay in region 1 but are radiated into region  $N$ , and finally on sheet  $A$  the fields decay in both regions 1 and  $N$ . Assuming that medium  $N$  is denser than medium 1 (e.g., if region 1 is air and region  $N$  soil), the path of integration is as shown in Fig. 2 on sheets  $D$ ,  $C$ , and  $A$ . The portion of the integral on sheet  $D$  represents the radiation spectrum of the source, at wavenumbers  $k_\rho$  for which radiation emanates into layers 1 and  $N$ ; after crossing the branch cut from sheet  $D$  to  $C$  the source is still in its radiation regime, but total internal reflection occurs at the interface of layers 1 and 2, such that the fields emanating into region 1 decay exponentially; finally, after crossing the branch cut to sheet  $A$ , the fields decay exponentially in both layers 1 and  $N$ , characteristic of total internal reflection at the top and bottom layers. The selected branch cuts and path of integration are similar to those in [37] for which there were only two Riemann sheets (two branch cuts) because the microwave structure of interest there was bound below by a conducting plane. However, in [37] the possibility of leaky-wave poles in quadrant one (and three) of the complex  $k_\rho$  was not mentioned. We have chosen a path of integration that resides above the finite number of surface- and leaky-wave poles in quadrant one (on the appropriate Riemann sheets), motivated by the pole positions in the limit  $\omega'' \rightarrow 0$ .

### C. Method of Complex Images at Complex Frequencies

To effect the method of complex images, we utilize the identity

$$\frac{e^{-jkR}}{4\pi R} = \frac{1}{2\pi} \int_0^\infty \frac{1}{j2k_z} e^{-jk \cdot /z - z'/J_0(k_\rho\xi)} k_\rho dk_\rho \quad (5a)$$

with

$$k^2 = k_\rho^2 + k_z^2, \quad R = \sqrt{(x - x')^2 + (y - y')^2 + |z - z'|^2} \quad (5b)$$

Therefore, to efficiently evaluate the integral in (3), for a

source in layer  $i$ , we form the approximation

$$\hat{f}(k_\rho, z, z') = \frac{e^{-jk_{zi}g(z, z')}}{j2k_{zi}} (\hat{h}k_\rho) \approx \frac{e^{-jk_{zi}(z, z')}}{j2k_{zi}} \cdot \left[ \lim_{k_\rho \rightarrow \infty} \hat{h}(k_\rho) + \sum_{m=1}^M a_m e^{-k_{zi}b_m} \right] \quad (6)$$

where the coefficients  $a_m$  and  $b_m$  are estimated along an appropriate line in the complex  $k_{zi}$  plane [22]–[25]. To this end, we change from integration in the variable  $k_\rho$  to integration in  $k_{zi}$ . The path of integration in the  $k_\rho$  plane of Fig. 2 is converted to a linear path in the complex  $k_{zi}$  plane (Fig. 3), along which parametric estimation of  $a_m$  and  $b_m$  can be readily effected. For simplicity, in Fig. 3 we only show the branch cuts in quadrants 1 and 4, in which the integration path resides; similar branch cuts exist for the negatives of the branch points shown. We have branch points at  $k_{zi} = \pm k_i$  due to  $k_\rho = [k_i^2 - k_{zi}^2]^{1/2}$ , at  $k_{zi} = \pm [k_i^2 - k_1^2]^{1/2}$  due to  $k_{z1} = [k_1^2 - k_i^2 + k_{zi}^2]^{1/2}$ , and at  $k_{zi} = \pm [k_i^2 - k_N^2]^{1/2}$  due to  $k_{zN} = [k_N^2 - k_i^2 + k_{zi}^2]^{1/2}$ . The branch cut emanating from  $k_{zi} = k_i$  has been selected such that  $\text{Im}(k_\rho) > 0$  over the entire linear path of integration (as it was over the entire path of integration in Fig. 2). The branch cuts emanating from  $[k_i^2 - k_1^2]^{1/2}$  and  $[k_i^2 - k_N^2]^{1/2}$  are selected as follows. In Fig. 3, along the solid path of integration starting at  $k_{zi} = k_i$ , we have  $k''_{z1} > 0$ ,  $k''_{zN} > 0$ , and  $k''_{zN} > 0$ , as for the initial path of integration on sheet  $D$  in Fig. 2. After this solid path of integration crosses the branch cut emanating from  $[k_i^2 - k_1^2]^{1/2}$ ,  $k''_{z1} > 0$ ,  $k''_{zN} < 0$ , and  $k''_{zN} > 0$ , and the dashed portion of integration represents the integration on sheet  $C$  of Fig. 2. Finally, after crossing the branch cut emanating from  $[k_i^2 - k_N^2]^{1/2}$ ,  $k''_{z1} > 0$ ,  $k''_{zN} < 0$ , and  $k''_{zN} < 0$ , and the dashed-dot path of integration in Fig. 3 represents integration on sheet  $A$  of Fig. 2. We perform the parametric fit in (6), using Prony's method [10], along the composite path in Fig. 3, which actually represents integration along three different  $k_{zi}$ -plane Riemann sheets. After so effecting the approximate representation on the right side of (6), the identity in (5a) is used to evaluate the space-domain Green's function analytically. We note that depending on the relative densities of layers 1,  $N$ , and  $i$ , the branch points may change their relative location and/or move into the fourth quadrant of the  $k_{zi}$ -plane, and similar branch cuts are realized (in Fig. 3 we assume layer  $i$  is denser than layer 1 (air) and layer  $N$ , with layer  $N$  also denser than layer 1).

#### D. Modifications Due to Lossy Media

The previous discussion was restricted to the case of lossless media (real-wave velocities), for the purpose of simplifying the analysis. However, for the case of targets buried in soil, losses must be accounted for. If the loss in layer  $N$  is sufficiently large, the spatial growth with  $|z|$  of the resonant fields in that layer will be overcome by the loss due to material dissipation and  $k_N$  will move into the fourth quadrant of the  $k_\rho$  plane (cf. Fig. 2). To achieve the same four Riemann surfaces as in Fig. 2 (dictated by the properties of  $k''_{z1}$  and  $k''_{zN}$ ), the branch cut associated with  $k_N$  is also in quadrant four (with the branch cut associated with its negative residing in quadrant two). Under

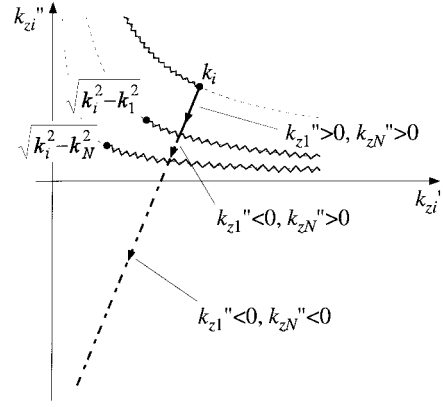


Fig. 3. Path of integration in the  $k_{zi}$  plane for source and observer in layer  $i$  (see Fig. 1). Along the solid path of integration  $k''_{z1} > 0$  and  $k''_{zN} > 0$  (characteristic of sheet  $D$  in Fig. 2), along the dashed path of integration  $k''_{z1} < 0$  and  $k''_{zN} > 0$  (characteristic of sheet  $C$  in Fig. 2), and along the dashed-dot path of integration  $k''_{z1} < 0$  and  $k''_{zN} < 0$  (characteristic of sheet  $A$  in Fig. 2).

this circumstance, we take the same general integration path as in Fig. 2, but only cross one branch cut (associated with  $k_1$ ). In this manner, we account for exponential growth of resonant fields into layer 1 (air) while realizing exponential decay in layer  $N$  (we only integrate on two Riemann sheets, as in [37], rather than integration on the three sheets considered in Fig. 2). Such modifications have straightforward implications with regard to integration in the  $k_{zi}$  plane (Fig. 3).

Therefore, when accounting for loss associated with real soils, care must be taken to track the location of the branch cuts (and poles) in the complex  $k_\rho$  and  $k_{zi}$  planes, but the general framework introduced in Sections II-B and C remains principally unchanged.

### III. EXAMPLE RESONANT-FREQUENCY COMPUTATIONS

Below we address the resonant behavior of several buried plastic targets, as computed by the algorithm outlined in Section II. Unfortunately, to our knowledge, there are no previous such computations existing in the literature (*measured* data have been presented [9], although these examples did not present sufficient details, e.g., soil properties, for numerical comparison). However, we have performed exhaustive tests on the accuracy of the results presented here, by carefully verifying, for example, the accuracy of the complex-image technique for Green's function evaluation at the complex (resonant) frequencies of interest.

In the first two examples, we consider a lossless cylindrical target of 8-cm diameter and 5-cm height, with dielectric constant  $\epsilon_{rB} = 20$ . This target is situated in a halfspace of clay, with electrical parameters of soil B described in Fig. 4 (representative of Puerto Rico clay with 10% water content, as reported in [38]). From Fig. 4, we see that the dielectric contrast between the target and soil background is significant, leading one to anticipate support of relatively high- $Q$  resonances. We consider this example first because the high- $Q$  resonance case is beset by less ambiguity in the soil electrical parameters. In particular, the frequency-dependent soil parameters in Fig. 4 are only valid on the *real*

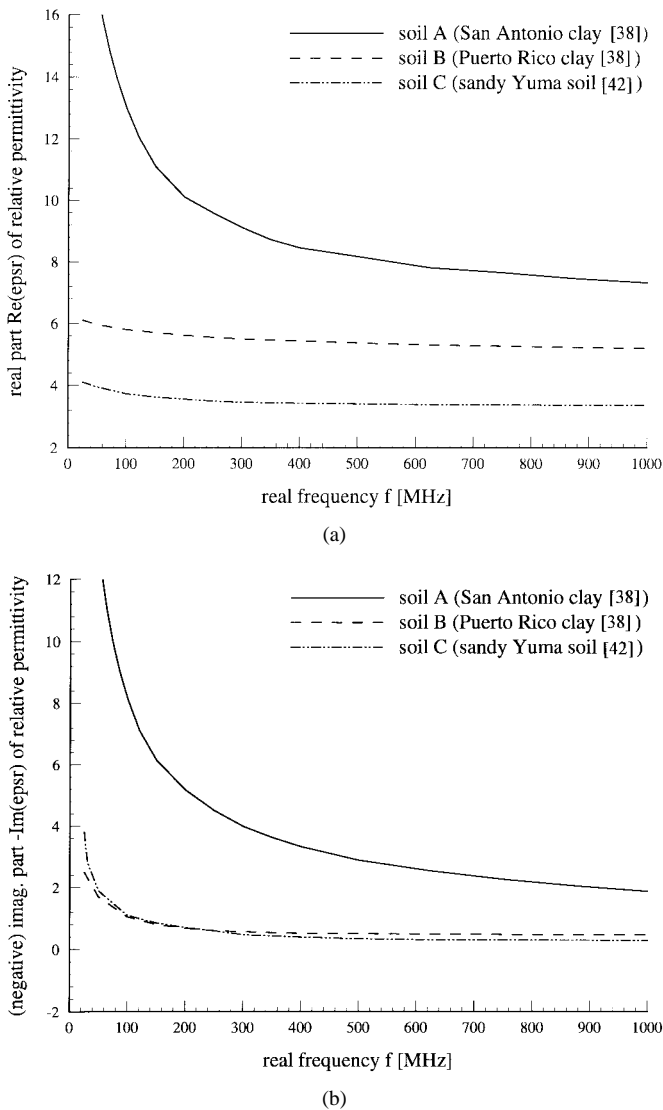


Fig. 4. Complex dielectric constant of three types of soil [38], [42] used in resonant-frequency computations. (a)  $\epsilon_r'$ . (b)  $\epsilon_r''$ .

frequency axis. One requires an analytic expression for the complex dielectric constant, valid at *all* frequencies to perform analytic continuation into the complex frequency plane [39]. Unfortunately, soil measurements are only performed over a very limited frequency band, undermining derivation of such an analytic function. Therefore, in the work presented here, the complex dielectric constant of the soil [needed in (1)] is set to the dielectric constant at  $\omega'$  (i.e., the real part of the complex resonant frequency). This approximation should be most appropriate for resonant frequencies near the real  $\omega$  axis ( $\omega''$  small relative to  $\omega'$ ), representative of the high- $Q$  resonant target we consider first.

In Fig. 5 we plot the resonant frequency of the fundamental mode as a function of depth from the top of the target, from 0.5 to 45 cm. In this plot, we also identify the resonant frequency of the same target situated in a homogeneous medium characterized by the same properties as the soil. As the target depth increases, one would anticipate that the resonant frequency would approach that of the same target in the homogeneous environment (i.e., that the air-soil interface will be of less

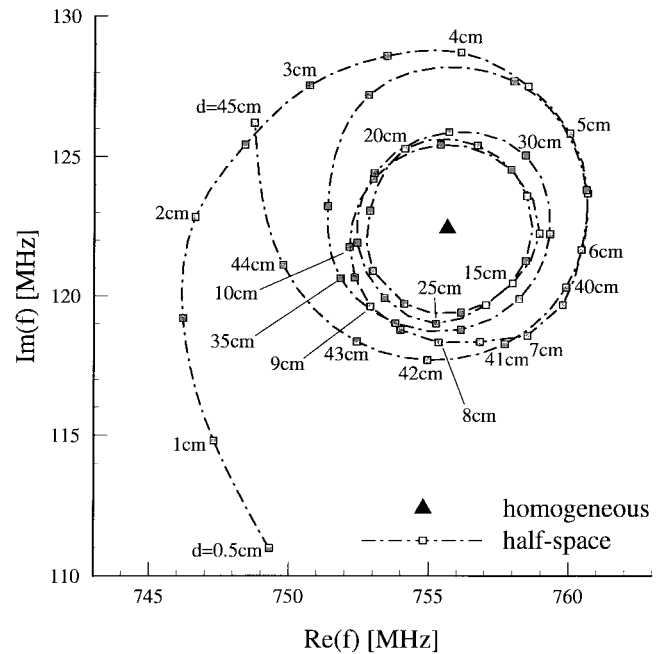


Fig. 5. Resonant frequency of a dielectric cylinder ( $\epsilon_r = 20$ ) of 8-cm diameter and 5-cm height buried in a half-space with electrical parameters described by soil B in Fig. 4. The resonant frequency is plotted as a function of depth  $d$  from the top of the target. Also plotted is the resonant frequency of the target situated in a homogeneous medium with the same electrical parameters.

importance with increasing target depth). We see in Fig. 5 that the buried-target resonant frequency does indeed approach that of the target in a homogeneous environment. However, an interesting spiraling effect is manifested with increasing target depth. A similar phenomenon has been witnessed for a wire above a lossy plane [40], a ring above a lossy halfspace [41], and for a wire buried in a lossy half-space [42]. All these examples, as well as the results in Fig. 5, can be explained in the same manner. In particular, assume that the target has (complex) resonant frequency  $\omega_1$  at depth  $d_1$ . If the target is lowered to a depth  $d_1 + n\lambda_1/2$ , where  $\lambda_1$  is the approximate resonant wavelength at  $\omega_1$  and  $n$  is an integer, the impedance seen by the target looking toward the air-ground interface is approximately unchanged (at frequency  $\omega_1$ ). Therefore, if the target resonates at frequency  $\omega_1$  for depth  $d_1$ , then it should also resonate at  $\omega_1$  for depths  $d_1 + n\lambda_1/2$ . Note that the resonant frequencies initially spiral inward (toward the homogeneous-medium resonance) with increasing depth, followed by a subsequent outward spiral. Similar effects were seen in [40]–[42] for perfectly conducting targets, with such attributed to mode coupling between the self modes of the target itself and “image” modes produced by reverberations between the target and the air-ground interface. We believe the results presented here are the first to show this effect also occurs for dielectric targets.

The algorithm in Section II allows computation of the resonant fields, in addition to the resonant frequencies of Fig. 5. As an example, in Fig. 6 we plot the resonant surface currents  $\mathbf{J}$  and  $\mathbf{M}$  of (1), representative of the tangential magnetic and electric fields, respectively, on the surface of the BOR target. For a set of depths considered in Fig. 5, we see

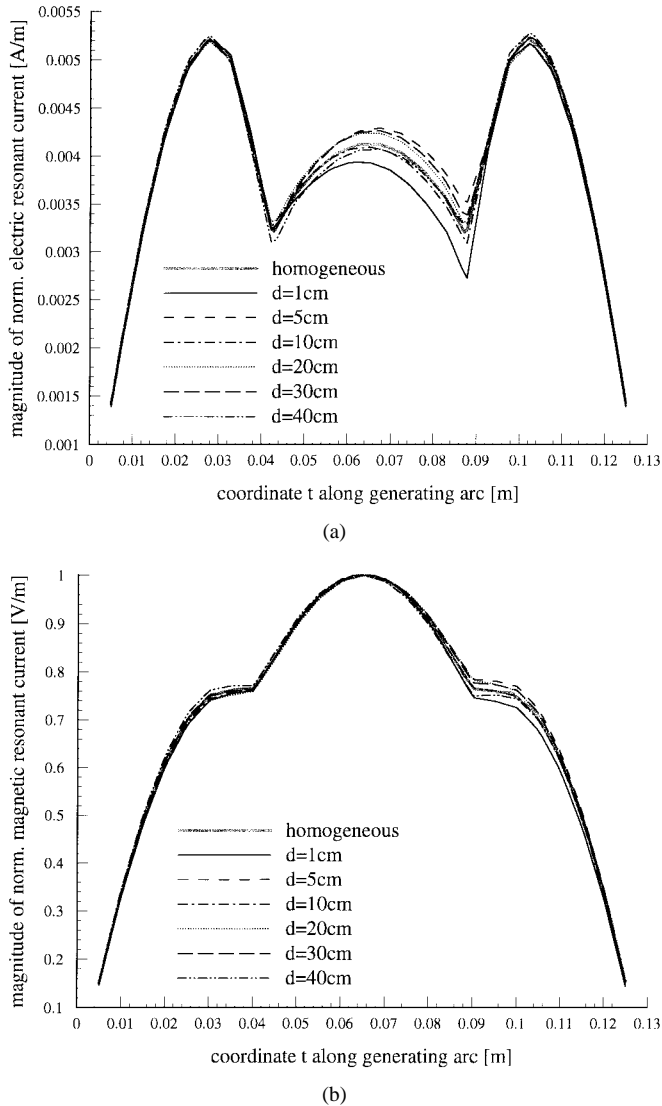


Fig. 6. Resonant currents  $\mathbf{J}$  and  $\mathbf{M}$  for the resonances in Fig. 5. (a) magnitude of  $J_\phi$ . (b) magnitude of  $M_t$ .

that there is minimal change in the resonant surface currents ( $J_\phi$  and  $M_t$  for the mode considered here) with increasing target depth. In Figs. 5 and 6 we have considered the properties of a single (lowest-order) resonant mode; an infinite set of higher-order modes exist [6].

To demonstrate an example of greater complexity than the half-space problem of Figs. 5 and 6, we consider the same target *centered* in a layer of thickness  $2d + 5$  cm (i.e., there is a distance  $d$  from the 5-cm-thick target to the top and bottom of the layer). Moreover, this layer of soil is characterized by the same electrical parameters as considered in Figs. 5 and 6 (soil type B in Fig. 4). Beneath this layer is a half-space characterized by soil type C in Fig. 4 (taken from [42], for 5% water content). This example may simulate a buried target, for which the disturbed soil has electrical parameters different than those of the background (undisturbed) soil. The resonant frequencies of this target are demonstrated in Fig. 7 for  $d$  ranging from 0.5 to 10 cm. For direct comparison, the corresponding results of the target in a half-space (Fig. 5) are also plotted. A spiraling behavior similar to that in Fig. 5 is

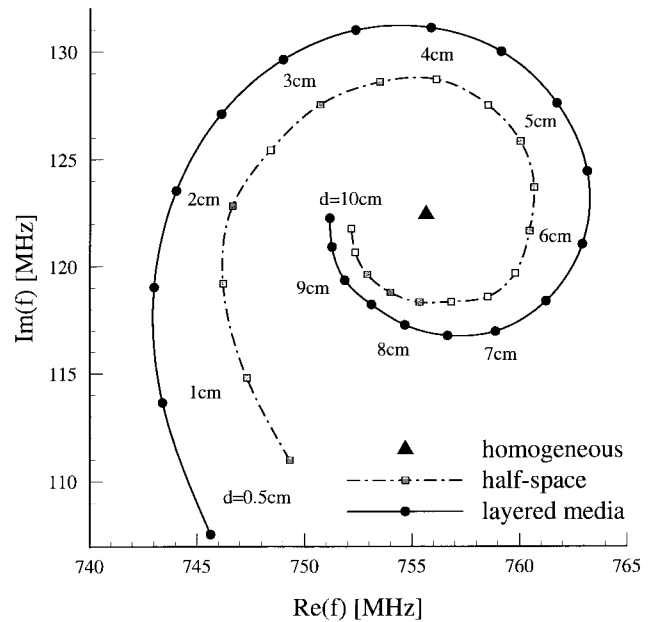


Fig. 7. Resonant frequency of the target considered in Fig. 5, centered in a layer of soil of thickness  $2d + 5$  cm, with the electrical properties of the layer described by soil B in Fig. 4. Beneath this layer of soil is a half-space with electrical properties described by soil C in Fig. 4. The target resonant frequency is plotted as a function of  $d$ . Also plotted is the resonant frequency of the target situated in a half-space environment (from Fig. 5) and in a homogeneous medium of soil B in Fig. 4.

manifested with increasing  $d$  with an analogous explanation. We see that the resonant frequencies are quantitatively very similar for these examples (for the same distance from the target to the air–soil interface). Moreover, note that the differences between the resonant frequencies diminishes as the distance from the target to both interfaces increases.

The examples in Figs. 5–7 considered a target of dielectric constant  $\epsilon_{rB} = 20$  such that relatively high- $Q$  resonances could be supported. As discussed, the approximations with regard to soil properties at complex frequencies are more appropriate under such circumstances. Nevertheless, most buried plastic targets of interest are composed of dielectric constants much smaller than considered above. We therefore consider an example using parameters that may be expected of practical radar problems. In particular, we consider a “PMN2” plastic antipersonnel mine, with dimensions shown in the inset of Fig. 8. This mine is principally plastic, with dielectric constant  $\epsilon_{rB} = 2.9$ . We consider this target buried in a half-space, using soil type A in Fig. 4. Because the electrical contrast between the target and background is now smaller than that considered in Figs. 5–7, one would anticipate this to be a lower  $Q$  target. The results in Fig. 8 are characterized by a spiraling behavior similar to that in Figs. 5 and 7. It is interesting to note that, for the depths considered here, the resonant frequencies of this target continually spiral outward with increasing depth (cf. Fig. 5).

#### IV. CONCLUSIONS

A rigorous method-of-moments (MoM) algorithm has been devised for modeling the resonances of targets buried in a lossy, layered medium, representative of soil. This research

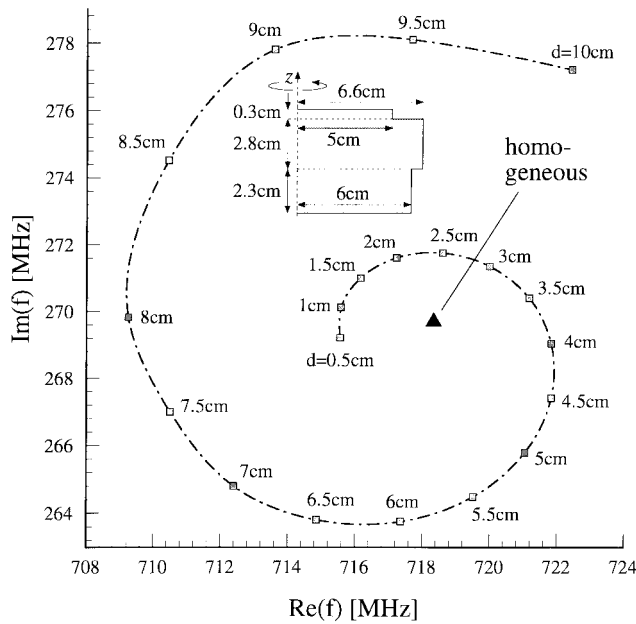


Fig. 8. Resonant frequency of a "PMN2" plastic land mine ( $\epsilon_{rB} = 2.9$ , with geometry shown inset) buried in a halfspace with electrical parameters described by soil type A in Fig. 4. Results are plotted as a function of depth  $d$  from the top of the target. For comparison, the resonant frequency of the target situated in a homogeneous medium of the same parameters is also plotted.

has been motivated by the use of resonances as discriminants for identifying buried plastic land mines. We have therefore restricted our analysis to the case of targets that can be simulated as a dielectric body of revolution since most plastic mines can be so approximated. Even with this simplification, such a MoM analysis is computationally challenging. In particular, one must evaluate the layered-medium Green's function at complex (resonant) frequencies. The layered-medium Green's function can only be expressed analytically in the spectral domain, with Sommerfeld-type integrals required for conversion to the space domain. Such integrals are computationally expensive if traditional integration techniques are employed and, therefore, here we have utilized the recently developed method of complex images [22]–[25].

The method of complex images is based on performing a parametric fit to the spectral Green's function along an appropriate path in the spectral domain, after which each term in the expansion can be converted to the space domain analytically via the Sommerfeld or Weyl identity [26]. While the method of complex images has been in use for several years, it is believed that this work is its first application to dielectric targets. We therefore required use of additional Green's function components than those used previously for purely perfectly conducting targets [21]–[25]. Moreover, the complex frequencies of interest required careful attention to the spectral-domain path of integration.

Several numerical examples have been presented. We initially considered relatively high-dielectric targets, for which high- $Q$  resonances are supported. Additionally, we also examined the lowest-order resonant frequency of an actual plastic land mine. It was demonstrated that the low electrical contrast between the soil and mine results in low- $Q$  resonances which undermine the utility of resonance-based discrimination.

## REFERENCES

- [1] C. E. Baum, "On the singularity expansion method for the solution of electromagnetic interaction problems," Air Force Weapons Lab. Interaction Notes, Note 88, 1971.
- [2] E. Heyman and L. B. Felsen, "A wavefront interpretation of the singularity expansion method," *IEEE Trans. Antennas Propagat.*, vol. AP-33, pp. 706–718, July 1985.
- [3] H. Shirai and L. B. Felsen, "Modified GTD for generating complex resonances for flat strips and disks," *IEEE Trans. Antennas Propagat.*, vol. AP-34, pp. 779–790, June 1986.
- [4] L. Marin, "Natural mode representation of transient scattered fields," *IEEE Trans. Antennas Propagat.*, vol. AP-21, pp. 809–818, Nov. 1973.
- [5] F. M. Tesche, "On the analysis of scattering and antenna problems using the singularity expansion technique," *IEEE Trans. Antennas Propagat.*, vol. AP-21, pp. 53–62, Jan. 1973.
- [6] B. L. Merchant, P. L. Moser, A. Nagl, and Überall, "Complex pole patterns of the scattering amplitude for conducting spheroids and finite-length cylinders," *IEEE Trans. Antennas Propagat.*, vol. 36, pp. 1769–1777, Dec. 1988.
- [7] E. J. Rothwell, J. Baker, K.-M. Chen, and D. P. Nyquist, "Approximate natural response of an arbitrary shaped thin wire scatterer," *IEEE Trans. Antennas Propagat.*, vol. 39, pp. 1457–1462, Oct. 1991.
- [8] L. Peters, Jr. and J. D. Young, "Applications of subsurface transient radars," in *Time-Domain Measurements in Electromagnetics*, E. K. Miller, Ed. New York: Van Nostrand Reinhold, 1986.
- [9] L. Peters, Jr., J. J. Daniels, and J. D. Young, "Ground penetrating radar as an environmental sensing tool," *Proc. IEEE*, vol. 82, pp. 1802–1822, Dec. 1994.
- [10] M. L. Van Blaricum and R. Mittra, "A technique for extracting the poles and residues of a system directly from its transient response," *IEEE Trans. Antennas Propagat.*, vol. AP-23, pp. 777–781, Nov. 1975.
- [11] D. G. Dudley, "Parametric modeling of transient electromagnetic systems," *Radio Sci.*, vol. 14, pp. 387–396, 1979.
- [12] Y. Hua and T. K. Sarkar, "Matrix pencil method for estimating parameters of exponentially damped/undamped sinusoids in noise," *IEEE Trans. Acoust., Speech, Signal Processing*, vol. 38, pp. 814–824, May 1990.
- [13] S. Vitebskiy and L. Carin, "Resonances of perfectly conducting wires and bodies of revolution buried in a lossy, dispersive half space," *IEEE Trans. Antennas Propagat.*, vol. 28, pp. 1575–1583, Dec. 1996.
- [14] J. M. Bourgeois and G. S. Smith, "A fully three-dimensional simulation of ground penetrating radar: FDTD theory compared with experiment," *IEEE Trans. Geosci. Remote Sensing*, vol. 34, pp. 36–28, Jan. 1996.
- [15] H. S. Chang and K. K. Mei, "Scattering of electromagnetic waves by buried and partly buried bodies of revolution," *IEEE Trans. Geosci. Remote Sensing*, vol. GRS-23, pp. 596–592, July 1985.
- [16] A. C. Dubey and R. L. Barnard, Eds., "Detection and remediation technologies for mines and minelike targets," *Proc. SPIE*, vol. 3079, 1997.
- [17] J. R. Wait, "Image theory of a quasistatic magnetic dipole over a dissipative half-space," *Electron. Lett.*, vol. 5, no. 13, pp. 281–282, June 1969.
- [18] Y. Rahmat-Samii, R. Mittra, and P. Parhami, "Evaluation of Sommerfeld integrals for lossy half-space problems," *Electromagn.*, vol. 1, no. 1, pp. 1–28, 1981.
- [19] S. F. Mahmoud and A. D. Metwally, "New image representations for dipoles near a dissipative earth," *Radio Sci.*, vol. 21, pp. 605–616, Nov. 1981.
- [20] I. V. Lindell and E. Alanen, "Exact image theory for the Sommerfeld half-space problem, Part III: General formulation," *IEEE Trans. Antennas Propagat.*, vol. AP-32, pp. 1027–1032, Oct. 1984.
- [21] K. A. Michalski and D. Zheng, "Electromagnetic scattering and radiation by surfaces of arbitrary shape in Layered media, Parts I and II," *IEEE Trans. Antennas Propagat.*, vol. 38, pp. 335–352, Mar. 1990.
- [22] J. J. Yang, Y. L. Chow, D. G. Fang, "Discrete complex images of a three-dimensional dipole above and within a lossy ground," *Proc. Inst. Elect. Eng.*, vol. 138, pt. H, no. 4, pp. 319–326, Aug. 1991.
- [23] R. M. Shubair and Y. L. Chow, "A simple and accurate complex image interpretation of vertical antennas present in contiguous dielectric half-spaces," *IEEE Trans. Antennas Propagat.*, vol. 41, pp. 806–812, June 1993.
- [24] Y. L. Chow, J. J. Yang, D. G. Fang, and G. E. Howard, "A closed-form spatial Green's function for the thick microstrip substrate," *IEEE Trans. Microwave Theory Tech.*, vol. 39, pp. 588–562, Mar. 1991.

- [25] S. Vitebskiy, K. Sturgess, and L. Carin, "Short-pulse scattering from buried perfectly conducting bodies of revolution," *IEEE Trans. Antennas Propagat.*, vol. 28, pp. 143–151, Feb. 1996.
- [26] W.C. Chew, *Waves and Fields in Inhomogeneous Media*. Piscataway, NJ: IEEE Press, 1995.
- [27] T. Tamir and A. A. Oliner, "Guided complex waves—Fields at an interface: Part I; Relation to radiation patterns: Part II," *Proc. Inst. Elect. Eng.*, vol. 110, pp. 310–334, 1963.
- [28] S. R. Vechinski and T. H. Shumpert, "Natural resonances of conducting bodies of revolution," *IEEE Trans. Antennas Propagat.*, vol. 38, pp. 1133–1136, July 1990.
- [29] A. W. Glisson, D. Kajfez, and J. James, "Evaluation of the modes in dielectric resonators using a surface integral equation formulation," *IEEE Trans. Microwave Theory Tech.*, vol. MTT-31, pp. 1023–1029, Dec. 1983.
- [30] S. Vitebskiy and L. Carin, "Resonances of perfectly conducting wires and bodies of revolution buried in a lossy dispersive halfspace," *IEEE Trans. Antennas Propagat.*, vol. 28, pp. 1575–1583, Dec. 1996.
- [31] N. Geng and L. Carin, "Wideband electromagnetic scattering from a dielectric BOR buried in a layered lossy, dispersive medium," *IEEE Trans. Antennas Propagat.*, vol. 47, pp. 610–619, Apr. 1999.
- [32] L. B. Felsen and N. Marcuvitz, *Radiation and Scattering of Waves*. Englewood Cliffs, NJ: Prentice-Hall, 1973.
- [33] N. K. Das and D. M. Pozar, "Full-wave spectral-domain computation of material, radiation and guided-wave losses in infinite multilayered printed transmission lines," *IEEE Trans. Microwave Theory Tech.*, vol. 39, pp. 54–63, Jan. 1991.
- [34] L. Carin and N. K. Das, "Leaky waves on broadside-coupled microstrip," *IEEE Trans. Microwave Theory Tech.*, vol. 40, pp. 58–66, Jan. 1992.
- [35] M. Tsuji and H. Shigesawa, "Packaging of printed circuit lines: A dangerous cause of narrow pulse distortion," *IEEE Trans. Microwave Theory Tech.*, vol. 42, pp. 1784–1790, Sept. 1994.
- [36] C. J. Madden, M. J. W. Rodwell, R. A. Marsland, Y. C. Pao, and D. M. Bloom, "Generation of 3.5 ps fall-time shock waves on a monolithic GaAs nonlinear transmission line," *IEEE Electron. Device Lett.*, vol. 9, p. 303, 1988.
- [37] K. A. Michalski and D. Zheng, "Analysis of microstrip resonators of arbitrary shape," *IEEE Trans. Microwave Theory Tech.*, vol. 40, pp. 112–119, Jan. 1992.
- [38] J. E. Hipp, "Soil electromagnetic parameters as functions of frequency, soil density, and soil moisture," *Proc. IEEE*, vol. 62, pp. 98–103, Jan. 1974.
- [39] K. E. Oughstun and G. C. Sherman, *Electromagnetic Pulse Propagation in Causal Dielectrics*. New York: Springer-Verlag, 1994, vol. 16.
- [40] L. S. Riggs and T. H. Shumpert, "Trajectories of singularities of a thin wire scatterer parallel to lossy ground," *IEEE Trans. Antennas Propagat.*, vol. AP-27, pp. 864–868, Nov. 1979.
- [41] E. J. Rothwell and M. J. Cloud, "On the natural frequencies of an annular ring above a conducting half space," *J. Electron. Waves Appl.*, vol. 10, pp. 155–179, Feb. 1996.
- [42] S. Vitebskiy, L. Carin, M. A. Ressler, and F. H. Le, "Ultra-wideband, short-pulse ground-penetrating radar: Simulation and measurement," *IEEE Trans. Geosci. Remote Sensing*, vol. 35, pp. 762–772, May 1997.

**Norbert Geng** (S'91–M'96) was born May 14, 1965 in Lauchringen, Germany. He received the Dipl.Ing. and Dr.Ing. degrees in electrical engineering from the University of Karlsruhe, Germany, in 1991 and 1996, respectively.

From 1991 to 1996, he was with the Institute for Microwaves and Electronics at the University of Karlsruhe, working on full-wave propagation modeling for radio communication systems. In January 1997 he joined the Department of Electrical and Computer Engineering at Duke University, Durham, NC, for 18 months, in a Visiting Postdoctoral capacity. Since July 1998 he has been back with the University of Karlsruhe. His current research interests include computational methods in electromagnetics and wave propagation modeling.

Dr. Geng received the Mannesmann Innovation Award in 1997 for his Ph.D. dissertation on full-wave propagation modeling for radio communication systems.

**David R. Jackson** (S'83–M'85–SM'95–F'99) was born in St. Louis, MO, on March 28, 1957. He received the B.S.E.E. and M.S.E.E. degrees from the University of Missouri, Columbia, in 1979 and 1981, respectively, and the Ph.D. degree in electrical engineering from the University of California, Los Angeles, in 1985.

From 1985 to 1991, he was an Assistant Professor in the Department of Electrical and Computer Engineering at the University of Houston, TX. From 1991 to 1998 he was an Associate Professor in the same department and since 1998 has been a Professor there. He is on the editorial board of the *International Journal of RF and Microwave Computer-Aided Engineering*. His current research interests include computer-aided design of microstrip antennas and circuits, microstrip antenna analysis and design, periodic structures, leaky-wave antennas, leakage effects in microwave integrated circuits, and bioelectromagnetics.

Dr. Jackson currently serves as the secretary for URSI United States Commission B and is a member of ADCOM for the IEEE Antenna and Propagation Society. He is on the editorial board of *IEEE TRANSACTIONS ON MICROWAVE THEORY AND TECHNIQUES*, is an Associate Editor for the IEEE Press Series on Electromagnetic Waves, and is a past Associate Editor for the *IEEE TRANSACTIONS ON ANTENNAS AND PROPAGATION*.

**Lawrence Carin** (SM'96) was born March 25, 1963 in Washington, DC. He received the B.S., M.S., and Ph.D. degrees, all in electrical engineering, from the University of Maryland, College Park, in 1985, 1986, and 1989, respectively.

In 1989, he joined the Electrical Engineering Department at Polytechnic University, Brooklyn, NY, as an Assistant Professor, and became an Associate Professor there in 1994. In September 1995 he joined the Electrical Engineering Department at Duke University, Durham, NC, where he is an Associate Professor. His current research interests include short-pulse scattering, propagation, and signal processing. He is the principal investigator on an Army Research Office funded Multidisciplinary University Research Initiative (MURI) on demining.

Dr. Carin is a member of the Tau Beta Pi and Eta Kappa Nu honor societies.